

Structural architecture of the 1980 Mount St. Helens collapse: An analysis of the Rosenquist photo sequence using digital image correlation

Thomas R. Walter

Department 2, Physics of the Earth, Helmholtz-Centre Potsdam, GFZ German Research Centre for Geosciences, Potsdam 14473, Germany

ABSTRACT

The collapse of Mount St. Helens (United States) on 18 May 1980 is one of the only incidents of its kind that was visually witnessed and instrumentally recorded. Previous analyses determined that the northern flank of the mountain failed, which resulted in a rockslide, and disintegrated during its mobilization to form a blocky facies and hummocky terrain in the downslope region. Gary Rosenquist's iconic photographs of the initial 18 May collapse were here analyzed by using a modern photogrammetric method to track portions of the moving flank across the photographs in the sequence. Thirty years after the 1980 Mount St. Helens rockslide, the digital image correlation technique enabled a precise investigation of the associated displacement vectors and strain. A listric basal detachment and several associated faults at the lateral edge of the rockslide were identified. In addition, the heterogeneous movements and a number of shear zones were detected within the sliding block, which had previously been assumed to be cohesive. The results of my study demonstrate the value of using optical images for strain analyses of active volcanoes—even decades after recording.

INTRODUCTION

The cataclysmic eruption of Mount St. Helens (United States) on 18 May 1980 included one of the most often studied lateral collapse events on a volcano. Close monitoring, sampling, and modeling allowed for the identification of eruption precursors and for the evacuation of the local population. The physical processes associated with the earthquake that triggered the collapse, the sector collapse, and the directed blast are well understood (Lipman and Mullineaux, 1981). Bulging of the north flank of the volcano at a horizontal velocity of 1.5–2.5 m/day was observed through the use of deformation measurements and visual inspections (Lipman et al., 1981). The earthquakes, steam eruptions, massive rockslide avalanche, and subsequent directed blast from the collapse provided important lessons for volcanologists, as did the destructive pyroclastic flows, mudflows, and floods that followed the event.

On 18 May 1980, amateur photographer Gary Rosenquist captured a set of photographs that is one of the most important data sources for understanding the Mount St. Helens collapse. Based on these images, previous studies have identified three main structural blocks (Lipman et al., 1981; Moore and Albee, 1981; Voight et al., 1981; Glicken, 1996). However, the transition of the slope from a three block proximal sequence (Fig. 1) to a largely disintegrated block facies and hummocky terrain at mid-distance (Glicken, 1996) is not well understood. The stage at which the initial blocks began to disintegrate and the locations of the sliding planes are also unclear. In this study, using an advanced digital image

correlation technique, I reanalyzed the Rosenquist photo sequence, focusing on the first sliding mass (block I; after Voight et al., 1981). As a result, a previously unobserved structural complexity that occurred during the first seconds of the evolving rockslide was identified.

ROSENQUIST PHOTO SEQUENCE

Gary Rosenquist was camping at a site near Bear Meadow (Fig. 1), located 17.5 km

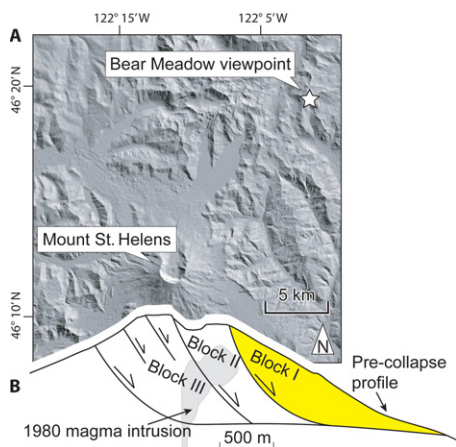


Figure 1. A: Shaded relief map of Mount St. Helens as it appeared after 18 May 1980 eruption. Gary Rosenquist took photographs of first seconds of 18 May rockslide avalanche at Bear Meadow viewpoint, which was 17.5 km from volcano. B: Schematic cross section (after Glicken, 1996) illustrates pre-eruption slope of Mount St. Helens and three main slide blocks. Focus of my study was on movement and disintegration of block I.

northeast of Mount St. Helens (46°18.813N, 122°02.205W). His camera was mounted on a tripod, and the first image of the “stable” (stable relative to the subsequent photographs) edifice was taken before the sector collapse. As soon as he recognized that the flank had begun to move, Rosenquist began taking the images of his famous photo sequence in a rapid succession. The geometry of the images and the focus of the photo sequence remained largely constant due to the use of a tripod, and this optical stability has allowed for a digital cross-correlation analysis. In total, 21 images showing the 18 May 1980 rockslide and eruption were captured. The initial condition was captured in two frames, in addition to the reference image, and four frames captured the early movement of block I.

Five images from the Rosenquist sequence were used in this work (frames a, b, c, d, and e from Voight, 1981), together with the reference image that was captured before the rockslide. These images show a volcano with a vertical axis of ~2000 m and a horizontal axis of ~4500 m. The rockslide of the northern volcano flank is visible in these images, and a compound of rock mass, glacier, snow avalanche, and dust is also visible (see Voight, 1981). Because the images that I used in my work were taken 30 yr ago on slide film, these images had to be converted from an analog format to a digital format. A standard scanner with unknown specifications was used for the analog-to-digital conversion (B. Voight, 2009, personal commun.). The regions that overlapped in all of the images were identified, and camera position instabilities corrected, using edges (Zitová and Flusser, 2003). The resolution of the overlapping regions was then defined in a regular grid matrix of 4756 × 2979 pixels, in which 1 pixel corresponded to ~10 m².

At the time the images were taken, the photographer attempted to directly record the timing of each picture in the sequence using a stopwatch, and the image timing was further evaluated based on the dynamic behavior of snow avalanches (Voight et al., 1981). Based on a reconstruction of the approximate timeline, it was determined that the entire photograph sequence was taken within a 28–49 s time interval and that the rockslide commenced between frames a and b at 15:32:21 (Universal Time) on

the morning of 18 May 1980 (Voight, 1981). The photo sequence timing was also explored in this study; however, as this paper only addresses the initial five frames, which were recorded during the first 3–4 s of the event (see Voight et al., 1981), the absolute timing did not appear to be accurate enough to warrant further interpretation. Therefore, the following work focused on the structural development of the rockslide rather than on its temporal development.

DIGITAL IMAGE CORRELATION

Digital image correlation (DIC) is a rapidly evolving technique for the computer-aided visual analysis of images. Photogrammetric cross-correlation analysis is a standard approach for detecting the features of an image; however, this method remains underused in volcanology research. Image cross-correlation was introduced in mechanics research more than 25 yr ago and has been used for structural analysis and materials deformation studies (Sutton et al., 1986). In the Earth sciences, this technique has been applied to a wide range of data sets (Sutton et al., 2009), including optical images (Johnson et al., 2008), panchromatic images (de Michele and Briole, 2007), and synthetic aperture radar amplitude values (Simons et al., 2002). Image correlation is a valuable tool for investigating time-dependent changes in observable properties, which may include local displacements and strains over various temporal and spatial scales. One of the main advantages of the image correlation technique is that the observed surface can be explored from a safe distance. Although the Rosenquist photos have been manually investigated previously, DIC allows for displacement detection with a resolution that is ~1 or 2 orders of magnitude greater than what is detectable by the human eye (Hauser and Walz, 2004). The general principle of DIC is based on the mathematical cross-correlation of a digital image data set that consists of a two-dimensional matrix of intensity values $I(U)$. The signal intensities at a given coordinate $U = (x, y)$ are recorded for two images that have similar optical parameters, such as the camera lens and the objective, viewing geometry, and illumination. In the simplest case, the shift between the images can be estimated by computing the perturbation of an image as a shifted copy of the reference image. For an image data set that consists of $n \geq 2$ images, the image intensity function $I(x, y, t)$ is given by the following equation (Horn and Schunck, 1981):

$$I(x, y, t) = (x + u, y + v, t + \delta t), \quad (1)$$

where (u, v) is the displacement over the time increment δt . The image matrix is divided into a grid of subregions; e.g., according to the method in Adrian (1991). Each subregion has a dimen-

sion of $N \times N$ and contains pixel information that is obtained from the two images; herein, one image is referred to as a master I_M , and the other image is referred to as the slave I_S , as illustrated in Figure 2. Given the near-constant image intensities,

$$\sum I_s^2(x + u, y + v), \quad (2)$$

the cross-correlation term allows for the quantification of the similarity between the subregions:

$$c(u, v) = \sum_{x=-n}^n \sum_{y=-n}^n I_M(x, y) I_S(x + u, y + v). \quad (3)$$

Various sophisticated DIC software packages are available. The results of this work were generated using DaVis, which is a well-tested package from LaVision (<http://www.lavision.de>). The Rosenquist images were investigated using StrainMaster, which is a state-of-the-art cross-correlation technique in the frequency domain. Using bicubic interpolation of the region in the vicinity of an integer peak (e.g., a bright pixel), the displacement vector can be obtained at a subpixel resolution, yielding a system resolution of 0.005 pixels. With higher resolutions,

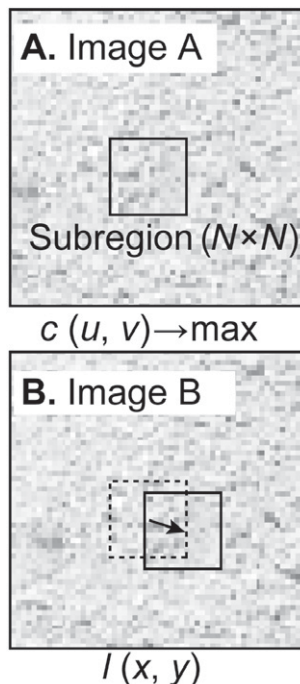


Figure 2. Illustration of digital image cross-correlation process (see text). A: Grayscale photograph was considered to be textured object with intensity values. B: In subsequent images, intensity at each subregion with dimensions of $N \times N$ was considered, and associated displacement was calculated based on correlation function equation.

the errors are larger in terms of accuracy and precision.

By using postprocessing pixel offset estimations and geometric scaling of the pixels to meters, the total and relative displacements can be obtained for any pixel, and the relative position and dislocation can be obtained with respect to neighboring observations. The latter estimation may allow for pixel grouping and for the estimation of the strain components (tension or shear), as elaborated in the following. The results of the Rosenquist photo sequence digital image correlation analysis presented here were processed by adaptively identifying the subregions, beginning with windows of 64×64 pixels and decreasing to areas of 16×16 pixels with a 50% overlap. Optical distortion errors and the effects that resulted from the two-dimensional representation of a three-dimensional event were ignored in this study, because a single camera was used for the photo sequence and the details about this camera equipment were no longer identifiable.

RESULTS

The displacement of the Mount St. Helens flank is shown as horizontal and vertical offset components, and the resulting vectors were used for the shear strain analysis. Geometric scaling was achieved according to the estimation of the volcano morphology before the collapse. The geometric and kinematic analyses were cross-checked and verified by comparison to previous results (Lipman et al., 1981; Moore and Albee, 1981; Voight, 1981).

The horizontal displacement (V_x) showed that the initial movement of block I was heterogeneous (Fig. 3). Greater V_x displacements were first observed at the mid-upper flank of block I (Fig. 3, B.2). The lower part of block I appeared to be kinematically separated from the upper part by a transition zone, in which little displacement occurred. During the progression of the rockslide (frames c, d, and e), the lateral displacement at the lower part of the block moved together with the upper part. The horizontal displacement within the initial images reached an approximate maximum of 680 m, in agreement with the ~700 m offset estimated by Voight (1981).

The vertical displacement values (V_y) showed that the main region of dislocation was located in the upper part of block I (Fig. 3B), whereas little vertical offset was observed in the lower section of this block. The V_y values reached 380 m in the first image pair and increased in amplitude slightly over time to 450 m.

Displacement vectors (Fig. 3C) were used to summarize the horizontal and vertical offsets and to further illustrate the heterogeneous displacement behavior of the moving flank. The strain field was visualized in terms of the

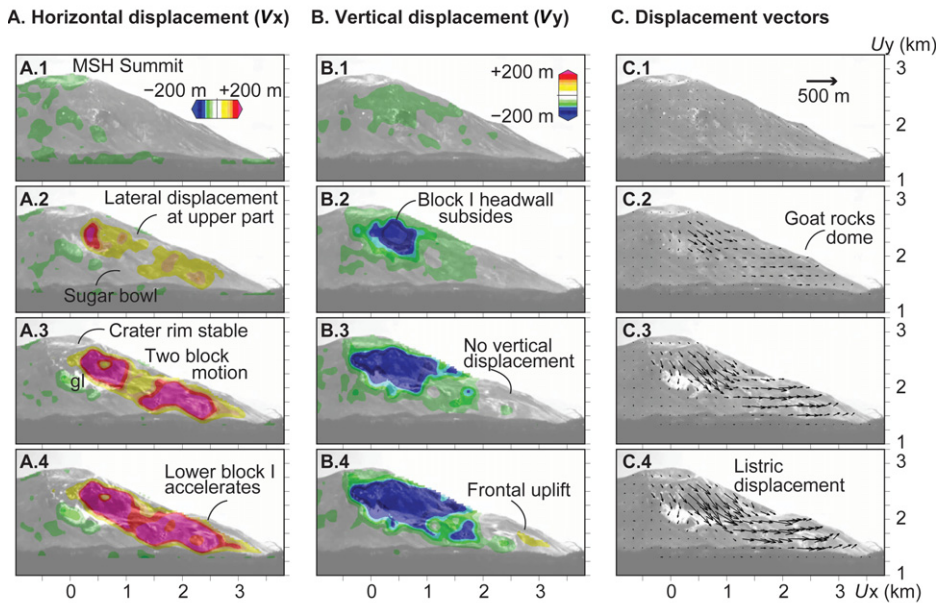


Figure 3. Displacement as observed by digital image correlation in first five images of Rosenquist photo sequence (see text). MSH—Mount St. Helens. **A:** Horizontal displacement (V_x); gl—Forsyth Glacier. **B:** Vertical displacement (V_y). Note that color scales are saturated. Maximum V_x was 680 m, and maximum V_y was 450 m. **C:** Displacement vectors. Note that all of the illustrations display displacements that are perpendicular to field of view. Displacement is shown in cumulative fashion, and background photos (1–4) are frames a–d in Voight (1981).

shear strain (Fig. 4A) and the maximum normal strain (Fig. 4B). The red contours in Figure 4A depict a clockwise (dextral) rotation, whereas the green to blue contours indicate the regions of counterclockwise (sinistral) shear strain. Assuming that the regions of shear strain depict the areas of the fault dislocations, the first main dextral faults developed at the mid-upper flank, which limited the area that was previously identified as the region with the greatest amount of

lateral movement (compared to that in Fig. 3). As the flank motion progressed, the individual segments of the dextral shear joined to form the detachment plane of the sector collapse. The last image pair showed that the slide area at the crater rim, which was referred to as block II by Voight (1981), began to move and was encircled upslope by a continuation of the shear plane. Sinistral rotations were generally observed at the upper limit of the flank, although the rela-

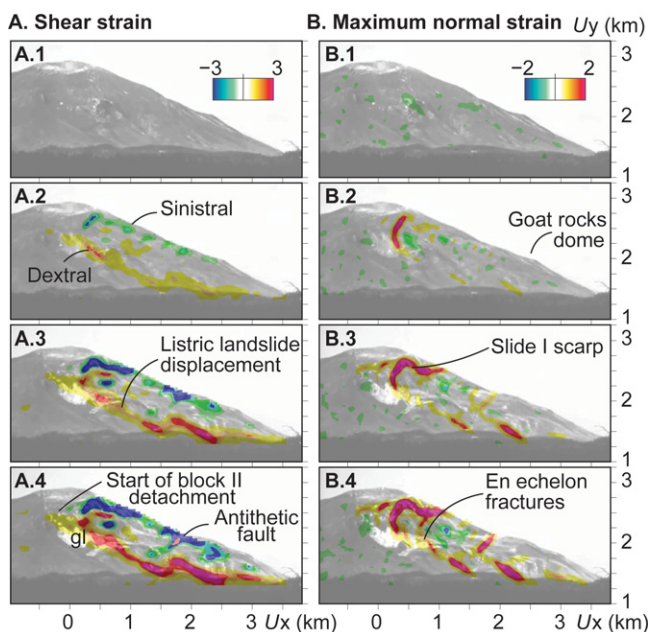


Figure 4. Cumulative strain field (see text). **A:** Second invariant of strain tensor (shear strain) (blue—sinistral rotation; red—dextral rotation) showing zones of likely shear faulting; gl—Forsyth Glacier. **B:** Maximum normal strain, extension (red) or compression (blue). Note that en echelon fractures and compression occurred at upper limit of Goat Rocks dome location. Strain is shown in cumulative manner, whereas background photos (1–4) are frames a–d from Voight (1981).

tionship of these rotations to the faulting activity remains unclear.

The maximum normal strain (Fig. 4B) is known to govern the inelastic behavior or failure (according to the maximum principal strain theory) and allows for a detailed investigation of the tensile fault components. Early horizontal strain was detected at the upper flank. This strain region was well expressed and exhibited an arch-shaped linear feature that may have allowed for the identification of the headwall of block I. During the continued flank motion, this extensional strain region increased in dimension and amplitude, and further segments developed downslope. The strain regions were initially isolated and were merged together in steps to form the main structural elements. The main detachment, which was the lateral limit of the slide, was expressed as a set of extensional shear zones that were arranged in an en echelon fashion. Moreover, the mid-flank had regions of high strain.

DISCUSSION AND CONCLUSION

I used the Rosenquist photos to analyze the complexity of the initial volcano sector collapse by using DIC. The DIC technique has several advantages; this technique is quantitative and is less biased by the user than standard visual inspection. Moreover, strain monitoring using a DIC analysis of photographs is a noninvasive full-field measurement, and therefore this method has the potential for a large number of applications. The limitations of a DIC analysis are mainly due to distortion or the presence of unstable optical parameters.

The structural interpretation of this data set indicated that strain localization commenced in the mid-upper flank and was associated with the formation of a localized landslide headwall that breached the surface. The same fault propagated downward to define block I, which began to slide both vertically and laterally. With progressive flank movement, additional smaller faults formed and merged to form a main listric landslide detachment zone. The mid-flank exhibited isolated points of high strain but was also a zone of kinematic transition from vertical to horizontal displacement vectors. The shear rotation and maximum strain analysis suggested that this zone hosted a left-lateral fault, which may have been connected to the deeper detachment fault. Therefore, the structural elements that were revealed by this analysis may provide novel insights into the disintegration of a rockslide avalanche in the immediate proximal region during the first seconds of motion.

The results of this work relied on images that show the beginning May 18 1980 rockslide avalanche, which then decapitated the magmatic system and triggered the explosive eruption (Voight, 1981). These results suggest that the disintegration of the block I occurred within the first 3–4 s

of the rockslide avalanche. The disintegration of block I was shown in three ways: using the heterogeneous vertical and horizontal displacement values, using shear and normal strain calculations. Specifically, the strain analysis indicated the occurrence of relatively well defined and isolated faults, which appeared as a combination of shear and dilatational slip planes.

The location of the most pronounced deformation, in terms of the displacement and strain, was in agreement with the location of the surface fissure development in the days prior to the 18 May rockslide avalanche (Moore and Albee, 1981). These surface fissures were located in the upper part of block I above and west of the Forsyth Glacier (gl in Figs. 3 and 4). Lower in this block, especially at the region of the maximum horizontal displacement, surface fissures were virtually absent, as noted by Moore and Albee (1981). Thus, the first seconds of the 1980 rock slide represented a structural change from the upper part to the lower part of block I. These two parts of this block were depicted by a near zero horizontal displacement at a position that was in agreement with the observed decrease of the vertical displacement values and a pronounced antithetic fault. This position was also in agreement with the region that was located nearby the Goat Rocks dome location. Samples from the dome have indicated that this structure was composed of fresh dacite that intruded a seventeenth to eighteenth century rock mass (Moore and Albee, 1981); this may indicate that this dome acted as a mechanical barrier during the movement of the rock mass. Therefore, this study suggests that block I was not a single block, and that it was a disintegrated rock mass that sheared internally and fractured before moving away from the source volcano.

The expression of the faults was more complex than previously ascertained. The main listric fault plane was partially in agreement with the detachment plane that had been noted before (Moore and Albee, 1981). The extent of the displacement was also in agreement with earlier findings. For example, Voight (1981) estimated 700 m of displacement, and I measured similar displacement at 680 m. In addition, this work revealed additional details about the type of the internal strain. The main detachment that limited the eastern (camera facing) side of the avalanche was defined by a set of en echelon subfeatures (Fig. 4, B.4), which were subjected to a high level of shear strain and to a locally high level of normal strain. Although theoretical landslides that are delimited by en echelon fault sets have been proposed (Muller and Martel, 2000), evidence of this phenomenon at Mount St. Helens has not been previously shown. Similarly, the proposal of a possible fault that separated

the upper and lower rockslide, with displacements and an orientation that were antithetic to the main detachment (Fig. 4, A.4), is novel for Mount St. Helens. Antithetic faults are known from other landslides, rollover anticlines, and experimental data (Le Corvec and Walter, 2009), hence supporting the finding at Mount St. Helens. In summary, the results of my work indicate that the Mount St. Helens rockslide avalanche was a more complex event than previously thought. In addition, this study provided evidence of structural elements that are characteristic of gravitational mass movements elsewhere at different scales.

DIC is a widely used technique in other engineering disciplines; however, its full capacity for deformation detection for volcanoes remains undervalued. The accurate detection of volcanic activity and of the dynamic developments that occur immediately prior to eruptions are among the main scientific results that are achieved using modern monitoring instrumentation (Dzurisin, 2007). The future analyses of volcano image sequences using modern DIC methods may allow for detailed structural and kinematic analyses. In recent years webcams and/or time-lapse digital cameras have been installed on numerous volcanoes, including Mount St. Helens, and may provide additional data sources for remotely operated strain field analyses.

ACKNOWLEDGMENTS

I thank Barry Voight for sharing the photo sequence analyzed, and the reviewers for constructive comments. Financial support was provided through the Helmholtz Centre Potsdam, GFZ German Research Centre for Geosciences.

REFERENCES CITED

- Adrian, R.J., 1991, Particle-imaging techniques for experimental fluid mechanics: Annual Review of Fluid Mechanics, v. 23, p. 261–304, doi:10.1146/annurev.fl.23.010191.001401.
- de Michele, M., and Briole, P., 2007, Deformation between 1989 and 1997 at Piton de la Fournaise Volcano retrieved from correlation of panchromatic airborne images: Geophysical Journal International, v. 169, p. 357–364, doi:10.1111/j.1365-246X.2006.03307.x.
- Dzurisin, D., 2007, Volcano deformation; geodetic monitoring techniques: Chichester, UK, Praxis Publishing, 441 p.
- Glicken, H., 1996, Rockslide-debris avalanche of May 18, 1980, Mount St. Helens Volcano, Washington: U.S. Geological Survey Open-File Report 96-677, 90 p.
- Hauser, C., and Walz, B., 2004, Bildbasierte Verformungsmessung mit der PIV-Methode: Geotechnik, v. 27, p. 339–343.
- Horn, B.K.P., and Schunck, B.G., 1981, Determining optical flow: Artificial Intelligence, v. 17, p. 185–203, doi:10.1016/0004-3702(81)90024-2.
- Johnson, J.B., Lees, J.M., Gerst, A., Sahagian, D., and Varley, N., 2008, Long-period earthquakes and co-eruptive dome inflation seen with particle image velocimetry: Nature, v. 456, p. 377–381, doi:10.1038/nature07429.

- Le Corvec, N., and Walter, T.R., 2009, Volcano spreading and fault interaction influenced by rift zone intrusions; insights from analogue experiments analyzed with digital image correlation technique: Journal of Volcanology and Geothermal Research, v. 183, p. 170–182, doi:10.1016/j.jvolgeores.2009.02.006.
- Lipman, P., and Mullineaux, D.R., eds., 1981, The 1980 eruptions of Mount St. Helens, Washington: U.S. Geological Survey Professional Paper 1250, 844 p.
- Lipman, P.W., Moore, J.G., and Swanson, D.A., 1981, Bulging of the north flank before the May 18 eruption; geodetic data, in Lipman, P., and Mullineaux, D.R., eds., The 1980 eruptions of Mount St. Helens, Washington: U.S. Geological Survey Professional Paper 1250, p. 143–155.
- Moore, J.G., and Albee, W.C., 1981, Topographic and structural changes, March–July 1980; photogrammetric data, in Lipman, P., and Mullineaux, D.R., eds., The 1980 eruptions of Mount St. Helens, Washington: U.S. Geological Survey Professional Paper 1250, p. 123–134.
- Muller, J.R., and Martel, S.J., 2000, Numerical models of translational landslide rupture surface growth: Pure and Applied Geophysics, v. 157, p. 1009–1038, doi:10.1007/s000240050015.
- Quinta da Fonseca, J., Mummery, P.M., and Withers, P.J., 2005, Full-field strain mapping by optical correlation of micrographs acquired during deformation: Journal of Microscopy, v. 218, p. 9–21, doi:10.1111/j.1365-2818.2005.01461.x.
- Simons, M., Fialko, Y., and Rivera, L., 2002, Co-seismic deformation from the 1999 M (sub w) 7.1 Hector Mine, California, earthquake as inferred from InSAR and GPS observations: Seismological Society of America Bulletin, v. 92, p. 1390–1402, doi:10.1785/0120000933.
- Sutton, M., Cheng, M., Peters, W.H., Chao, Y.J., and McNeill, S.R., 1986, Application of an optimized digital correlation method to planar deformation analysis: Image and Vision Computing, v. 4, p. 143–150, doi:10.1016/0262-8856(86)90057-0.
- Sutton, M.A., Ortu, J.-J., and Schreier, H.W., 2009, Image correlation for shape, motion and deformation measurements: Basic concepts, theory and applications: New York, Springer, 364 p.
- Voight, B., 1981, Time scale for the first moments of the May 18 eruption, in Lipman, P., and Mullineaux, D.R., eds., The 1980 eruptions of Mount St. Helens, Washington: U.S. Geological Survey Professional Paper 1250, p. 69–86.
- Voight, B., Glicken, H., Janda, R.J., and Douglass, P.M., 1981, Catastrophic rockslide avalanche of May 18, in Lipman, P., and Mullineaux, D.R., eds., The 1980 eruptions of Mount St. Helens, Washington: U.S. Geological Survey Professional Paper 1250, p. 347–377.
- Zitová, B., and Flusser, J., 2003, Image registration methods: A survey: Image and Vision Computing, v. 21, p. 977–1000, doi:10.1016/S0262-8856(03)00137-9.

Manuscript received 24 February 2011

Revised manuscript received 15 March 2011

Manuscript accepted 22 March 2011

Printed in USA